ACCSCIENCE PUBLISHING

Explora: Environment and Resource

ORIGINAL RESEARCH ARTICLE

Nickel foam-supported nickel–cobalt layered double hydroxide/platinum composite electrocatalyst for ammonia oxidation reaction

Xinyu Zhao, Xinyue Wang*, Hongli Cai, Jialu Liu, Jiali Gu, Yingying Zhao, and Liang Zhang*

Department of Chemistry, College of Chemistry and Materials Engineering, Bohai University, Jinzhou, Liaoning, China

Abstract

With increasing interest in direct ammonia fuel cells, designing and developing high-activity electrocatalysts for the electrochemical ammonia oxidation reaction has become a critical research focus. In this work, a nickel foam-supported nickel–cobalt layered double hydroxide/platinum composite (Pt-NiCo-LDH) was synthesized through electrochemical deposition and displacement reactions for enhanced electrocatalytic activity. Key synthesis parameters, including reaction temperature and chloroplatinic acid hexahydrate ($H_2PtCl_6 6H_2O$) concentration, were systematically optimized. Electrochemical characterization using cyclic voltammetry revealed that the optimal catalyst – synthesized in a solution containing 450 μL deionized water and 1,050 μL 0.1 moL/L $H_2PtCl_6{\cdot}6H_2O$ at 20°C for 8 h – showed an oxidation peak current of 154.60 mA and a low onset potential of –0.38 V (versus mercury/mercury oxide), indicating exceptional catalytic activity. The support of nickel foam provided favorable conditions to deposit NiCo-LDH nanowires, providing sites for the growth of platinum nanoparticles, thus promoting the catalytic activity of the Pt-(NiCo-LDH) electrocatalyst.

Keywords: Electrocatalyst; Ammonia oxidation reaction; Nanocomposite; Platinum; Nickel–cobalt layered double hydroxide

***Corresponding authors:**
Xinyue Wang (wangxinyue@qymail.bhu.edu.cn)
Liang Zhang (zhangliang1@qymail.bhu.edu.cn)

Citation: Zhao X, Wang X, Cai H, *et al*. Nickel foam-supported nickel–cobalt layered double hydroxide/platinum composite electrocatalyst for ammonia oxidation reaction. *Explora Environ Resour.* 2025;2(3):025170033. doi: 10.36922/EER025170033

Received: April 23, 2025

Revised: June 6, 2025

Accepted: June 9, 2025

Published online: June 30, 2025

1. Introduction

With the continuous consumption of fossil fuels, the development and application of clean energy sources have received increasing attention.[1-3] Among these, hydrogen is considered one of the ideal energy carriers.[4] However, currently, hydrogen is primarily produced from fossil fuels, which is accompanied by the generation and emission of carbon dioxide. In addition, the application of hydrogen is also limited by challenges related to storage and transportation.[5] In contrast, ammonia, owing to its high energy density, rich hydrogen content, and low safety risks, has garnered significant attention.[6] On one hand, decomposing ammonia into nitrogen (N_2) and hydrogen can address the problems associated with hydrogen storage and transportation. On the other hand, the electrochemical oxidation reaction of ammonia can be applied to remove ammonia nitrogen in water bodies – thereby addressing environmental issues – and for the design and development of direct ammonia fuel cells.[7,8] The combustion of direct ammonia

fuel cells produces only water as a byproduct, making it an extremely clean fuel.

Considerable research efforts have focused on electrocatalysts for the ammonia oxidation reaction (AOR). Among noble metals, platinum (Pt) showed the best electrocatalytic activity compared to others. Various morphologies of pure Pt, including cubic Pt,[9] sheet-like Pt,[10] and flower-like Pt,[11] have been reported as catalysts for the electrochemical AOR. These different morphologies can be achieved by controlling the electrodeposition potentials and using surfactants. In addition, to further improve AOR activity, research has extended to certain Pt-based binary and ternary electrocatalysts. Vooys *et al.*[12] established the nitrogen adsorption strength trend as follows: Ruthenium > rhodium > palladium > iridium > Pt >> gold, silver, and copper.[12] Therefore, Pt-based alloys, including Pt-nickel (Ni), Pt-iridium, and Pt-gold, have been synthesized, showing superior electrocatalyst performance compared to pure Pt. In addition, certain oxides, such as yttrium oxide,[13] stannic oxide,[14] and cerium oxide,[15] have also been used to modify Pt. For example, cerium oxide-modified Pt showed better AOR performance, including lower onset potential and higher oxidation peak current, compared to pure Pt.

In regard to transition metals and their oxides/oxyhydroxides, Ni has been regarded as a promising candidate for AOR electrocatalysts. However, challenges remain, such as the compromised long-term stability of Ni due to corrosion during ammonia electrolysis. To overcome these issues, various Ni-based materials have been developed, including Ni–copper alloys,[16] copper oxide/Ni hydroxide,[17] Ni–copper oxyhydroxide,[18] Ni–copper–iron oxyhydroxide,[19] and Ni–cobalt (Co) layered double hydroxides. These materials aim to control the electron structure and the adsorption of ammonia. For example, Ren *et al.*[20] synthesized copper oxide/Ni through a one-step replacement reaction and used charge density difference and Mulliken charge analyses to explain the enhanced electrocatalytic performance.[20] Wang *et al.*[21] developed a boron-modified Ni–iron layered double hydroxide (NiFe-LDH) supported on Ni foam (NF), where boron nanoclusters served as charge bridges to regulate electron redistribution in NiFe-LDH and expose more active metal sites.[21]

In this work, to fabricate a high-performance electrocatalyst for AOR, NiCo-LDH nanowires were first electrodeposited onto NF, followed by the growth of Pt nanoparticles through a galvanic replacement reaction. The ratio of chloroplatinic acid hexahydrate ($H_2PtCl_6{\cdot}6H_2O$), reaction time, and reaction temperature were systematically controlled, and the resulting samples were characterized. In addition, the samples were analyzed using scanning electron microscopy (SEM; ZEISS 300, HITACHI, Japan) and X-ray photoelectron spectroscopy (XPS; ESCALAB 250XI, Thermofisher, USA).

2. Methodology

2.1. The synthesis of nickel–cobalt layered double hydroxide/platinum composite

2.1.1. Pre-treatment of nickel foam

The NF was first cut into thin sheets measuring 10 mm × 25 mm × 1 mm. The sheets were then placed into a 50 mL beaker and immersed in 3 mol/L hydrochloric acid for 10 min. Next, the NF was transferred to ethanol (analytical reagent grade; Tianli Chemical Reagent Company, China) and sonicated for 10 min. Finally, the NF was washed with deionized water and dried in an oven (Shangcheng Instrument Manufacturing Company, China) at 50°C for later use. The resulting sample is referred to as NF.

2.1.2. Preparation of nickel–cobalt layered double hydroxide

First, 0.571 g of Ni(II) chloride hexahydrate (analytical reagent grade; Shanghai Macklin Biochemical Co., Ltd. China) and 0.195 g of Co(II)chloride hexahydrate (analytical reagent grade: Shanghai Macklin Biochemical Co., Ltd. China) were added into 50 mL of deionized water and stirred to form a homogeneous solution. Subsequently, 0.30 g of urea (analytical reagent grade; Shanghai Macklin Biochemical Co., Ltd. China) was added to the aforementioned mixed solution, followed by magnetic stirring for an hour to ensure complete homogenization. The resultant mixture and a cleaned NF substrate were transferred into a 100 mL teflon-lined stainless-steel autoclave (Wanruigude Company, China), which was then sealed and maintained at 120°C for 12 h in an electric oven (Shangcheng Instrument Manufacturing Company, China). After naturally cooling to room temperature, the obtained sample was collected, rinsed, and denoted as NiCo-LDH.

2.1.3. Preparation of platinum–(nickel–cobalt layered double hydroxide)

Nickel–cobalt layered double hydroxide was placed into 4 mL centrifuge tubes. Then, 150 μL, 300 μL, 450 μL, and 600 μL of $H_2PtCl_6{\cdot}6H_2O$ (0.1 mol/L) (analytical reagent grade; Shanghai Macklin Biochemical Co., Ltd. China) were added into the centrifuge tubes along with 1,350 μL, 1,200 μL, 1,050 μL, and 900 μL of deionized water, respectively, to obtain a solution with a volume of 1,500 μL. The mixtures were placed in a water bath at 20°C for 8 h. The obtained Pt-(NiCo-LDH) samples were labeled as Pt-(NiCo-LDH)-X (X = 1, 2, 3, 4). Under the optimal

concentration of 450 μL of $H_2PtCl_6 \cdot 6H_2O$ (0.1 moL/L) and 1,050 μL of deionized water, the temperature of the water bath was controlled at 30°C, 40°C, and 50°C, with heating maintained for 8 h. The obtained samples were named as Pt-(NiCo-LDH)-X (X = 5, 6, 7). In addition, the sample prepared without $H_2PtCl_6 \cdot 6H_2O$ (0.1 moL/L) was named NiCo-LDH-8, the sample prepared without NiCo-LDH was named Pt-NF-9, and the NF was designated NF-10. Figure 1 shows the synthesis process of NiCo-LDH and Pt-(NiCo-LDH)-X.

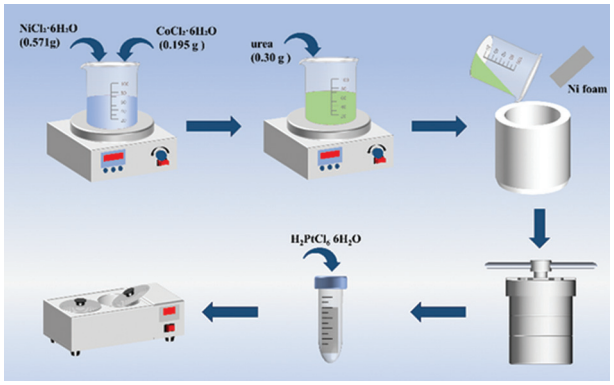

Figure 1. The synthesis process of nickel (Ni)–cobalt layered double hydroxide and platinum–(Ni–cobalt layered double hydroxide)-X

3. Results and discussion

In this work, ammonium chloride (NH_4Cl) was used as the ammonia source. The cyclic voltammetry (CV) technique was employed to analyze the electrochemical reactions based on the peak current, peak potential, and related parameters.[22] The oxidation peak current is one of the important parameters to evaluate the activity of catalysts. Higher peak currents indicate better catalytic activity, characterized by faster electron transfer, accelerated electrode reaction rates, and lower reaction resistance. To select the best synthesis condition of the catalyst, the CV technique was conducted on all catalysts for the AOR. The oxidation reaction peak currents were collected and used as a key parameter to evaluate the catalyst activity. In addition, to obtain an electrocatalyst with excellent catalytic performance, the volume of H_2PtCl_6 $6H_2O$ and the reaction temperatures of H_2PtCl_6 $6H_2O$ and NiCo-LDH were regulated.

First, the concentrations of H_2PtCl_6 $6H_2O$ were studied. Figure 2A-D shows the CV curves of the Pt-(NiCo-LDH)-X (X = 1, 2, 3, 4) catalysts synthesized with H_2PtCl_6 $6H_2O$ volumes ranging from 0.15 mL to 0.60 mL. In the 1 M potassium hydroxide (KOH) and 1 M KOH + 0.1 M NH_4Cl solutions, a distinct oxidation peak emerged at

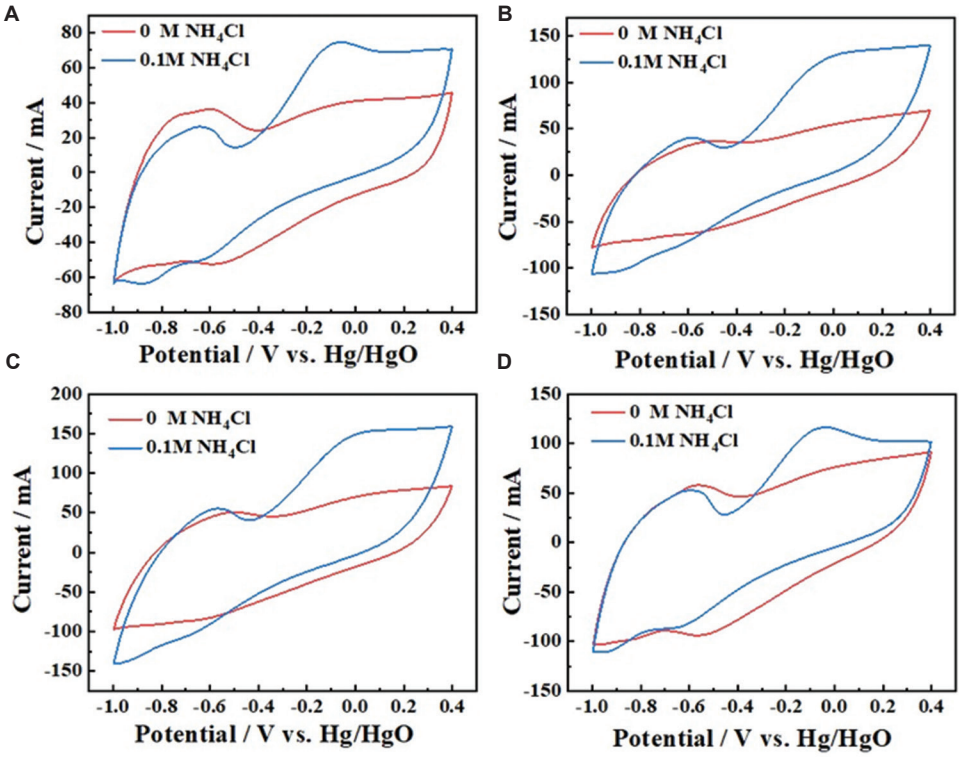

Figure 2. The cyclic voltammetry curves of platinum–(nickel–cobalt layered double hydroxide)-X (Pt-[NiCo-LDH]-X). (A) Pt-(NiCo-LDH)-1, (B) Pt-(NiCo-LDH)-2, (C) Pt-(NiCo-LDH)-3, and (D) Pt-(NiCo-LDH)-4 catalysts in 1 M potassium hydroxide (KOH) and 1 M KOH + 0.1 M ammonium chloride (NH4Cl) solutions. Hg/HgO refers to mercury/mercury oxide used as the reference.

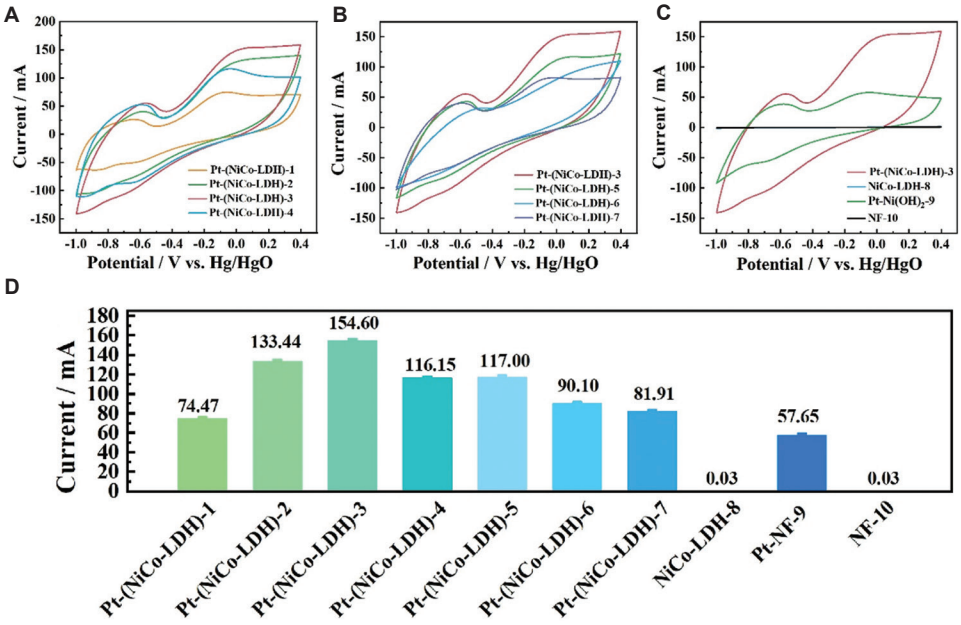

Figure 3. The cyclic voltammetry curves of (A) platinum–(nickel–cobalt layered double hydroxide) (Pt-[NiCo-LDH]-X) (X = 1, 2, 3, 4), (B) Pt-(NiCo-LDH)-X (X = 3, 5, 6, 7), (C) Pt-(NiCo-LDH)-3, NiCo-LDH-8, Pt-Ni foam (NF)-9, and NF-10 catalysts in the mixed solution of 1 M potassium hydroxide and 0.1 M ammonium chloride, and (D) the oxidation peak currents of all catalysts. Hg/HgO refers to mercury/mercury oxide used as the reference.

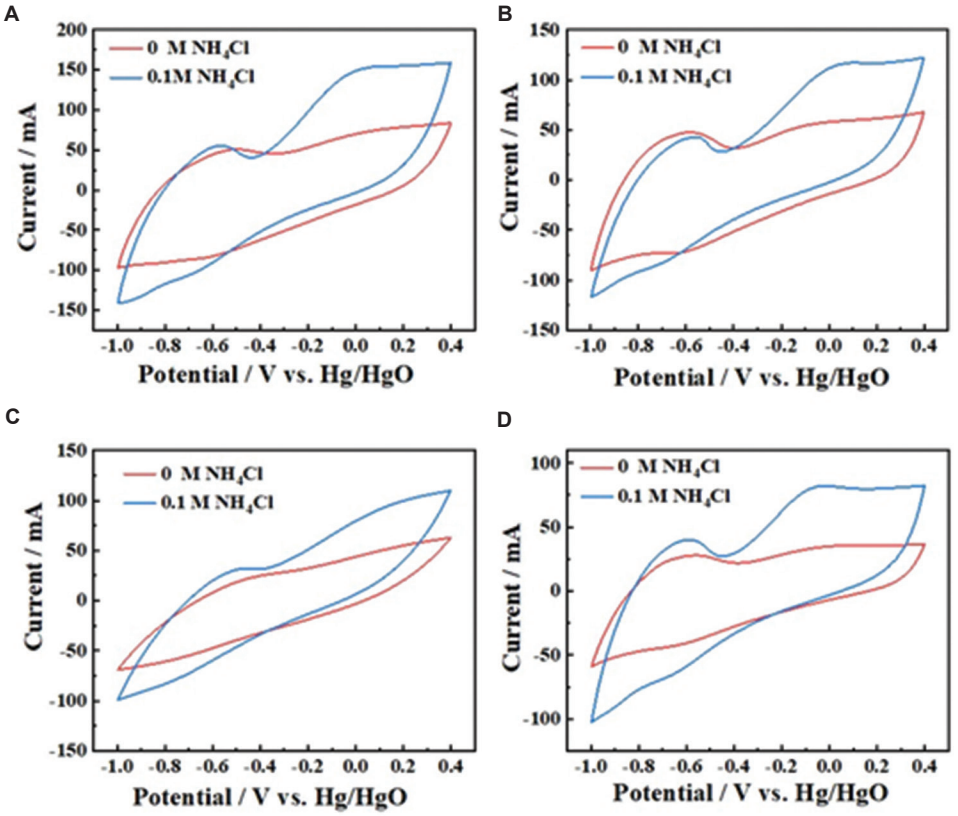

Figure 4. The cyclic voltammetry curves of platinum–(nickel–cobalt layered double hydroxide)-X (Pt-[NiCo-LDH]-X). (A) Pt-(NiCo-LDH)-3, (B) Pt-(NiCo-LDH)-5, (C) Pt-(NiCo-LDH)-6, and (D) Pt-(NiCo-LDH)-7 catalysts in 1 M potassium hydroxide (KOH) and 1 M KOH + 0.1 M ammonium chloride (NH4Cl) solutions. Hg/HgO refers to mercury/mercury oxide used as the reference.

approximately −0.05 V. Figure 3A shows the CV curves of Pt-(NiCo-LDH)-1, Pt-(NiCo-LDH)-2, Pt-(NiCo-LDH)-3, and Pt-(NiCo-LDH)-4 catalysts in the mixed solution of 1 M KOH and 0.1 M NH_4Cl, with oxidation peak currents shown in Figure 3D. Notably, with an increasing volume of H_2PtCl_6 $6H_2O$, the oxidation peak current exhibited a notable upward trend, escalating from 74.47 mA to 154.60 mA, indicating an enhanced catalytic activity. However, at 0.6 mL, the catalytic activity of Pt-(NiCo-LDH)-4 decreased significantly to an oxidation peak current of 116.15 mA. This indicated that during the displacement process between $PtCl_6^{2-}$ and Co^{2+}, a large quantity of Co^{2+} was consumed, and excessive H_2PtCl_6 $6H_2O$ may have destabilized the NiCo-LDH structure, thereby resulting in the loss of catalytic activity.

Based on the addition of 0.45 mL of H_2PtCl_6 $6H_2O$, the reaction temperature (20°C, 30°C, 40°C and 50°C) between H_2PtCl_6 $6H_2O$ and NiCo-LDH was further controlled. Figure 4 shows the CV curves of the Pt-(NiCo-LDH)-X (X = 3, 5, 6, 7) catalysts in 1 M KOH and 1 M KOH + 0.1 M NH_4Cl solutions. Figure 3B shows the CV curves of Pt-(NiCo-LDH)-X (X = 3, 5, 6, 7) catalysts in the mixed solution of 1 M KOH and 0.1 M NH_4Cl. As shown in Figure 3B, as the reaction temperature increased, the oxidation peak current gradually decreased. The oxidation peak currents decreased from 154.60 mA to 81.91 mA (Figure 3D), indicating that the catalytic activity gradually weakened. Increasing reaction temperatures accelerated the rate of the displacement reaction between $PtCl_6^{2-}$ and Co^{2+}. Simultaneously, the nucleation rate of Pt was also accelerated, which hindered the formation of highly dispersed Pt and reduced the number of catalytically active sites.

To demonstrate that Pt-(NiCo-LDH)-3 exhibited better catalytic activity than NF, NiCo-LDH, and Pt-NF, the catalytic activities of NiCo-LDH-8, Pt-NF-9, and NF-10 were also tested in 1 M KOH and 1 M KOH + 0.1 M NH_4Cl solutions, as shown in Figure 5. No discernible variation in current was observed in the CV curves of NiCo-LDH-8 and NF-10, indicating that pure NiCo-LDH and NF did not show obvious catalytic activity in this measurement system. In contrast, the Pt-NF-9 catalyst exhibited a clear oxidation peak with an oxidation peak current of 57.65 mA, indicating that the Pt showed electrocatalytic activity. In addition, the oxidation peak current of Pt-(NiCo-LDH)-3 was 2.7 times that of Pt-NF-9, indicating that there is a good synergistic effect between NiCo-LDH and Pt. Table 1 shows the electrocatalytic activities of some reported

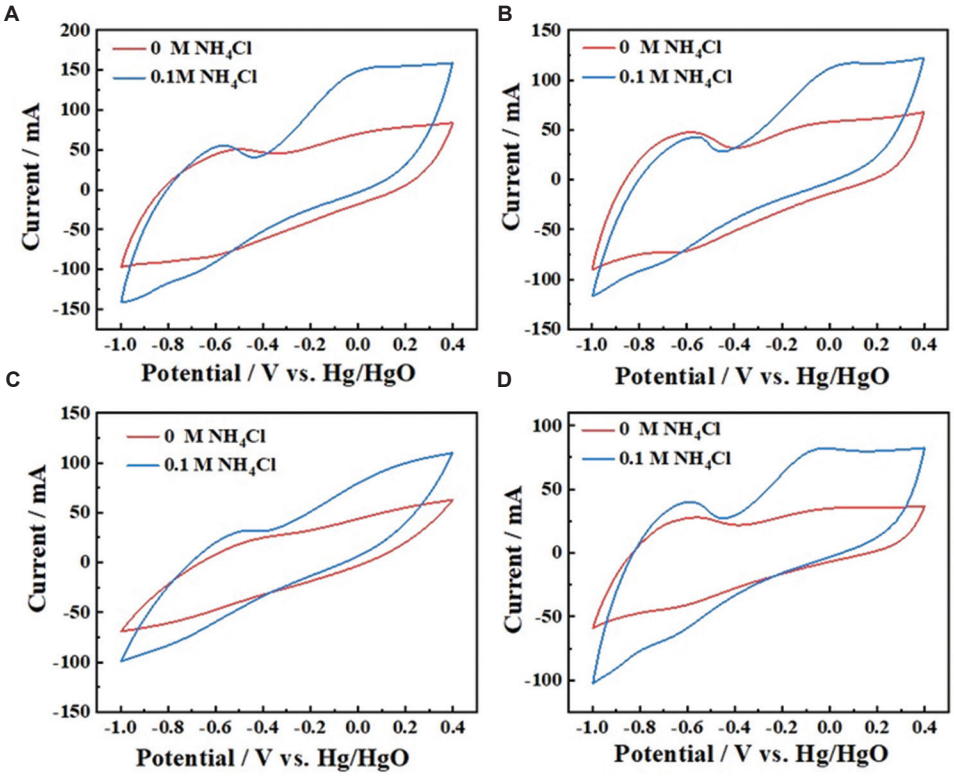

Figure 5. The cyclic voltammetry curves of (A) platinum–(nickel–cobalt layered double hydroxide)-3 (Pt-[NiCo-LDH]-X), (B) NiCo-LDH-8, (C) Pt-Ni foam (NF)-9, and (D) NF-10 catalysts in 1 M potassium hydroxide (KOH) and 1 M KOH + 0.1 M ammonium chloride (NH4Cl) solutions. Hg/HgO refers to mercury/mercury oxide used as the reference.

catalysts. Compared to these catalysts, the onset potential and current density of Pt-(NiCo-LDH)-3 were accepted.

To find the optimal potential ranges of Pt-(NiCo-LDH)-3 for AOR, different potential ranges, including −1 – 0.4 V, −0.8 – 0.6 V, −0.6 – 0.8 V, −0.4 – 1.0 V, and −0.2 – 1.2 V, have been selected and measured for the electrocatalytic test. As shown in Figure 6A-D, with the rightward shift of the potential window, the oxidation peak around −0.05 V gradually decreased and eventually disappeared, whereas the oxidation peak at around 0.7 V gradually became increasingly prominent. This shift occurred because moving the potential window to the right gradually deviated from the suitable operating potential of the Pt catalyst, revealing the potential range more suitable for NiCo-LDH. However, as shown in Figure 4C and D, the catalytic activity of NiCo-LDH alone was not significant, and the current change before and after the addition of NH_4Cl was minimal. These results indicate that the catalytic activity of Pt-(NiCo-LDH)-3 mainly originated from Pt, with the most suitable operating window range being −1 – 0.4V.

To investigate the kinetics of AOR on the Pt-(NiCo-LDH)-3 surface, CV curves were recorded at scan rates ranging from 20 to 200 mV/s, as shown in Figure 7A. With increasing scan rates, the oxidation peak currents increased accordingly. Figure 7B shows the relationship between

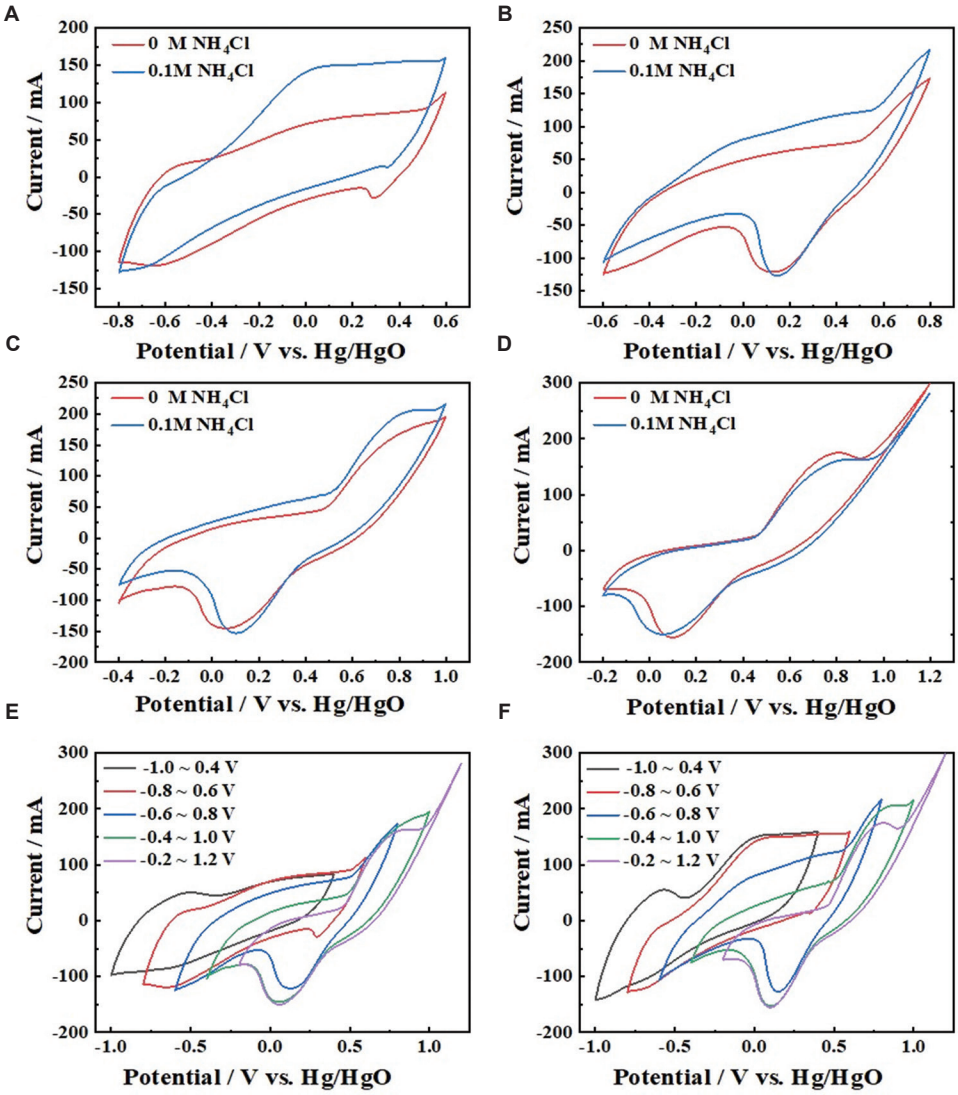

Figure 6. The potential ranges for ammonia oxidation reaction in (A, B, C and D) 1 M potassium hydroxide (KOH) and 1 M KOH + 0.1 M ammonium chloride (NH_4Cl) solutions. The cyclic voltammetry curves of different potentials (E) in 1 M KOH and (F) in 1 M KOH + 0.1 M NH_4Cl solution. Hg/HgO refers to mercury/mercury oxide used as the reference.

Table 1. The ammonia oxidation reaction test conditions and activity of reported catalysts

Electrode	Onset potential (V)	Current density (mA/cm^2)	Electrolyte	Stability	References
Platinum/cobalt–iron/nickel foam	−0.019 V_{RHE}	50.00 at 0.029 V_{RHE}	0.2 M $N_2H_4^+$ 1.0 M KOH	At −0.017 V_{RHE} for 100 h	23
Platinum–iridium–copper	0.350 V_{RHE}	40.60 at 0.500 V_{RHE}	0.1 M NH_3^+ 1.0 M KOH	At 0.650 V_{RHE} for 500 s	24
Silver/iron (II) oxide/titanate nanotubes	−0.500 $V_{Ag/AgCl}$	-	0.1 M NH_4Cl^+ 1.0 M phosphate-buffered saline	At −0.250 $V_{Ag/AgCl}$ for five cycles	25
Platinum–cobalt hydroxide–nickel foam-3	0.250 V_{RHE}	10.17 at − 0.200 V_{RHE}	0.1 M NH_4Cl^+ 1.0 M KOH	-	31
Nickel–copper–sulfur treated/carbon paper	1.374 V_{RHE}	110.00 at 1.690 V_{RHE}	0.2 M NH_4Cl^+ 1.0 M NaOH	At 1.640 V_{RHE} for 24 h	27
Platinum–iridium (5:5 atomic ratio)/XC-72	0.350 V_{RHE}	32.20 at 0.500 V_{RHE}	1.0 M ammonia$^+$ 1.0 M KOH	At 0.500–1.000 V_{RHE} for 4,000 cycles	28
Platinum–(nickel–cobalt layered double hydroxide)-3	−0.03 $V_{Hg/HgO}$	154.60 at 0.24 $V_{Hg/HgO}$	0.1 M NH_4Cl^+ 1.0 M KOH	At 0.24 $V_{Hg/HgO}$ for 5,000 s	This work

Abbreviations: Ag: Silver; AgCl: Silver chloride; Hg: Mercury; HgO: Mercury oxide; KOH: Potassium chloride; NH_4Cl: Ammonium chloride; RHE: Reversible hydrogen electrode.

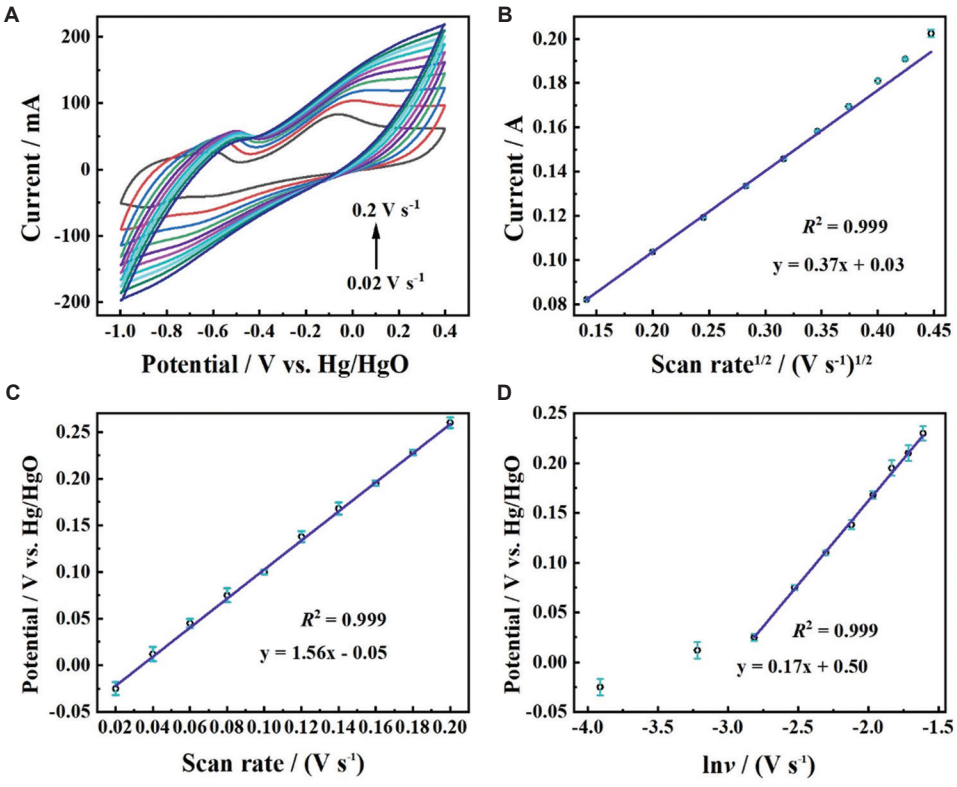

Figure 7. Cyclic voltammetry curves of platinum–(nickel–cobalt layered double hydroxide)-3 electrode in 1 M potassium hydroxide + 1 mM ammonium chloride at different scan rates. (B) Oxidation peak current densities versus (vs.) the square root of the scan rates. (C) Oxidation peak potentials vs. scan rate. (D) The effect of scan rate on peak potentials. Hg/HgO refers to mercury/mercury oxide used as the reference.

oxidation peak currents and scan rates. Based on the fitted curve, a favorable linear correlation was observed between the oxidation peak currents and the square root of the scan rate, described by the linear equation: y = 0.37x+0.03 (R^2 = 0.999), indicating a diffusion-controlled process. Moreover, with the increase in scan rates, the oxidation peak potential (Epa) demonstrated a subtle positive shift. In addition, a strong linear correlation was established

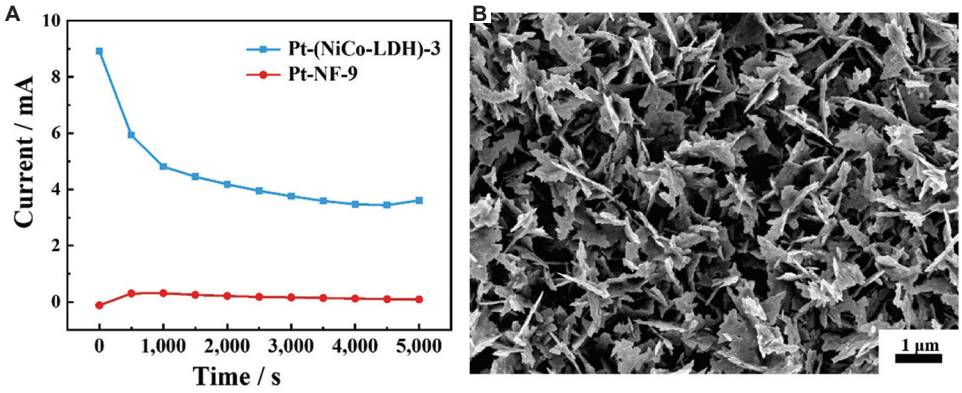

Figure 8. The stability measurement and SEM image after stability measurement of Pt-(NiCo-LDH)-3. (A) The stability measurements of platinum–(nickel–cobalt layered double hydroxide) (Pt-[NiCo-LDH]-3) and Pt-nickel foam (NF)-9. (B) The scanning electron microscopic image of Pt-(NiCo-LDH)-3 after use. Scale bar: 1 μm, magnification: 10.00 KX.

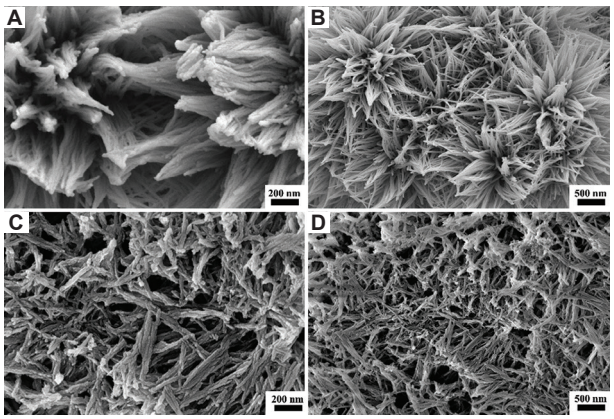

Figure 9. Scanning electron microscopy images. (A and B) Nickel–cobalt layered double hydroxide (NiCo-LDH) and (C and D) platinum-(NiCo-LDH)-3. Scale bars: 200 nm and 500 nm, magnifications: 200 nm (50.00 K), and 500 nm (20.00 K).

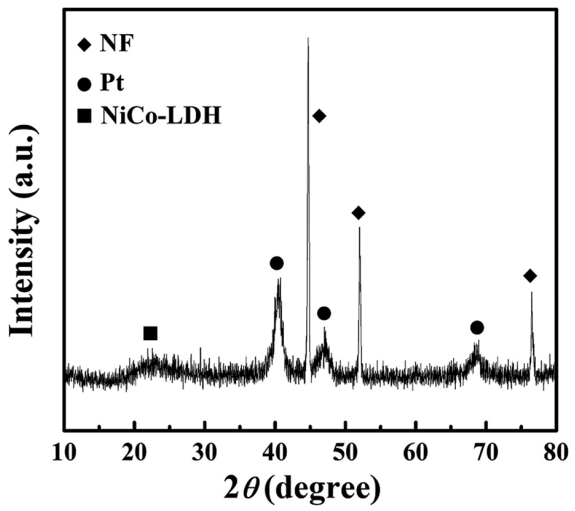

Figure 10. The X-ray diffraction pattern of platinum Pt-(NiCo-LDH)-3 Abbreviations: NF: Nickel foam; NiCo-LDH: Nickel–cobalt layered double hydroxide; Pt: Platinum.

between the Epas and the scan rates ($R^2 = 0.999$) (Figure 7C). This finding suggested the presence of an irreversible process for AOR on the Pt-(NiCo-LDH)-3 electrode. A good linear relationship was observed between the Epa and the logarithm of the scan rate (ln ν) (ν ≥ 0.06 V/s), as shown in Figure 7D. Laviron's theoretical model[29] was employed to fit the data, resulting in Equation I. Based on this fitting, the number of electrons (n) participating in the rate-determining step of the AOR on the Pt-(NiCo-LDH)-3 electrode can be calculated.

$$E_{Pa} = E^{\theta} + \left(\frac{RT}{\alpha nF}\right)\ln\left(\frac{RTk^{\theta}}{\alpha nF}\right) + \left(\frac{RT}{\alpha nF}\right)\ln\nu \quad \text{(I)}$$

The parameters in Equation I were Faraday's constant (F = 96,485 C/mol), temperature (T = 298.15 K), gas constant (R = 8.314 J/[K·moL]), standard electrode potential (E^{θ}), and electron transfer coefficient (α). The standard rate constant is denoted as k^{θ}. The αn value was determined by the slope of the E_{Pa} versus ln ν as 0.15. Meanwhile, the value of α can be computed by Equation II:

$$E_{Pa} - E_{P/2} = 1.857\left(\frac{RT}{\alpha F}\right) \quad \text{(II)}$$

In Equation II, $E_{p/2}$ is the potential of the half peak. The α was calculated as 0.25, and the number of transfer electrons in the rate-determining step of AOR was determined as 0.6.

To evaluate the stability of the catalyst, stability tests were conducted on Pt-(NiCo-LDH)-3 and Pt-NF-9. The results, shown in Figure 8, indicate that Pt-(NiCo-LDH)-3 has a higher current and exhibits better catalytic stability than Pt-NF. After the stability test, Pt-(NiCo-LDH)-3 maintained its sheet-like morphology.

Three analyses, SEM, X-ray diffraction (XRD, D8 advance, Bruker, Germany), and XPS, were employed to study the morphology and composition of Pt-(NiCo-LDH)-3. Figure 9A and B show the SEM images of NiCo-LDH. It was observed that NiCo-LDH existed in the form of nanowires, with a certain degree of agglomeration. At a lower magnification (Figure 9B), it was easy to observe that these nanowires combined to form a flower-like morphology. However, after the growth of Pt after incubation in the water bath, the flower-like structure formed by the agglomeration of these NiCo-LDH nanowires degraded, as shown in Figure 9C and D. This could be attributed to two aspects: first, the addition of H_2PtCl_6 $6H_2O$ introduces a large number of H^+, which provides a certain corrosive effect on NiCo-LDH, and second, the Co^{3+} ions within NiCo-LDH dissolve out and act as reducing agents to convert $PtCl_6^{2-}$ to Pt. Unfortunately, the presence of Pt could not be clearly identified from the SEM images of Pt-(NiCo-LDH)-3. In addition, compared to the SEM image of Pt-(NiCo-LDH)-3 after use, the nanowire of Pt-(NiCo-LDH)-3 showed more apparent changes, indicating that the NiCo-LDH underwent phase transitions and lattice rearrangements during the electrochemical measurement process.

Figure 10 exhibits the XRD pattern of Pt-(NiCo-LDH)-3. As shown in Figure 7, the three strong diffraction peaks at 44.7°, 52.0°, and 76.5° could be attributed to NF. In addition, three diffraction peaks could be detected at 40.5°, 47.1°, and 68.7°, attributable to the 111, 200, and 220 crystal planes of Pt.[30] In addition, a weaker diffraction peak of NiCo-LDH was observed at 22.8°.[24] The XRD diffraction peaks of NiCo-LDH and Pt confirm the successful growth of NiCo-LDH and Pt on the surface of NF.

To further characterize the chemical composition of Pt-(NiCo-LDH)-3, XPS was performed, and the corresponding results are presented in Figure 11. Figure 11A revealed four deconvoluted peaks in the Ni 2p. The peaks at 856.14 eV and 873.81 eV correspond to Ni^{2+} $2p_{3/2}$ and Ni^{2+} $2p_{1/2}$, respectively,[30] whereas the satellite peaks at 861.73 eV and 880.43 eV are attributed

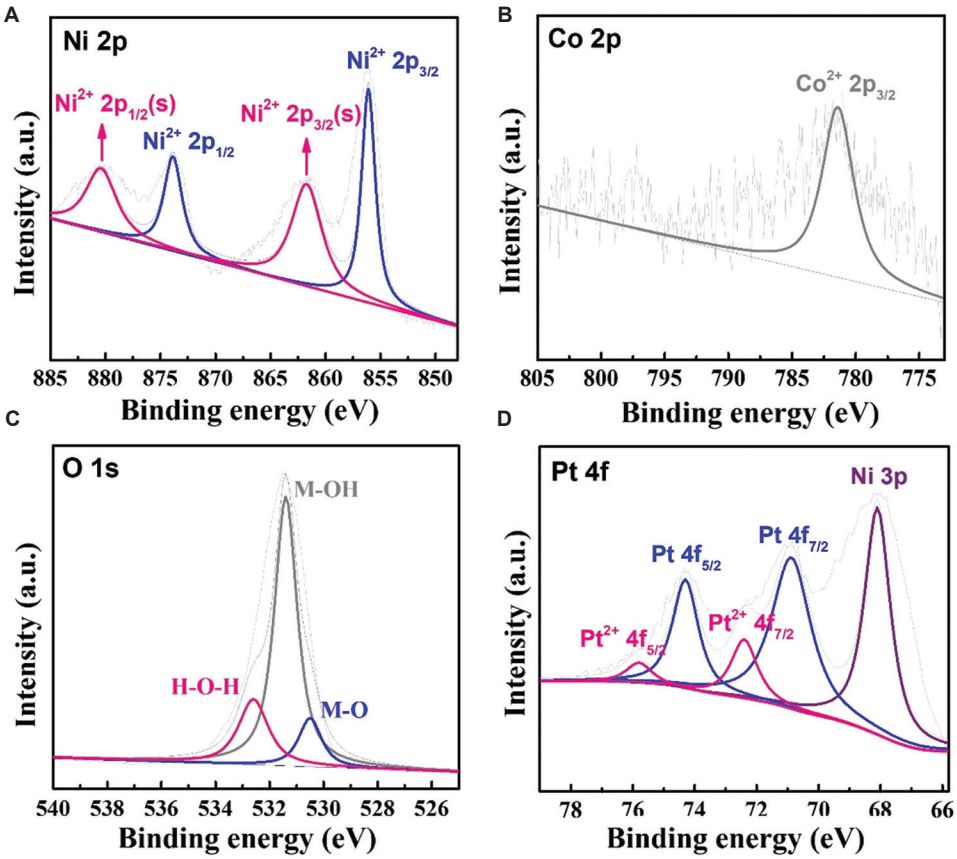

Figure 11. The X-ray photoelectron spectroscopy spectra of (A) nickel (Ni) 2p, (B) cobalt (Co) 2p, (C) oxygen (O) 1s, and (D) platinum (Pt) 4f in Pt-(NiCo layered double hydroxide)-3

to shake-up processes. In Figure 11B, the Co 2p spectrum exhibits a prominent peak at 781.42 eV, assigned to Co^{2+} $2p_{3/2}$.[31] For the oxygen 1s spectrum (Figure 11C), three peaks at 530.52 eV, 531.44 eV, and 532.5 eV were resolved, corresponding to lattice oxygen (M-O), hydroxyl groups (M-OH), and adsorbed water (H-O-H), respectively.[31] Collectively, these XPS results confirm the successful formation of NiCo-LDH. Finally, the XPS spectrum of the Pt is shown in Figure 11D. Two peaks at 70.87 eV and 73.31 eV could be attributed to Pt $4f_{7/2}$ and Pt $4f_{5/2}$, indicating that Pt was zero-valent. In addition, the fitted peak at 68.10 eV could be ascribed to Ni 3p.[30] These results indicated that Pt nanoparticles have been deposited onto NiCo-LDH.

4. Conclusion

This study successfully developed a high-performing Pt-(NiCo-LDH) supported by NF through a solvothermal reaction and displacement reaction. All samples' catalytic activities for AOR were measured. Among the prepared samples, Pt-(NiCo-LDH)-3 exhibited superior electrocatalytic activity, with an oxidation peak current of 154.60 mA and a low onset potential of −0.38 V (versus mercury/mercury oxide). The excellent electrocatalytic activity was mainly attributed to good synergistic effects; NiCo-LDH nanowires provided a large specific surface area, offering favorable conditions for the growth of Pt, while Pt showed good catalytic activity in the electrochemical oxidation of ammonia. This work presents a potential catalyst for the AOR in direct ammonia fuel cells.

Acknowledgment

None.

Funding

This work was supported by the Innovation Training Program for College Students of Bohai University (202410167039).

Conflict of interest

The authors declare that they have no competing interests.

Author contributions

Conceptualization: Xinyue Wang, Jiali Gu, Liang Zhang
Investigation: Xinyu Zhao, Hongli Cai, Jialu Liu
Methodology: Liang Zhang, Yingying Zhao
Writing – original draft: Xinyue Wang, Liang Zhang
Writing – review & editing: Xinyue Wang, Liang Zhang

Ethics approval and consent to participate

Not applicable.

Consent for publication

Not applicable.

Availability of data

Data will be made available upon request to the corresponding author.

References

1. Wang YJ, Wang R, Tanaka K, *et al*. Global spatiotemporal optimization of photovoltaic and wind power to achieve the Paris agreement targets. *Nat Commun*. 2025;16(1):2127.

   doi: 10.1038/s41467-025-57292-w

2. Wuttke A, Bagger A. Predicting electrocatalytic urea synthesis using a two-dimensional descriptor. *Commun Chem*. 2025;8(1):30.

   doi: 10.1038/s42004-025-01424-2

3. Shen Y, Fang N, Liu X, *et al*. Observation of metal-organic interphase in cu-based electrochemical co_2-to-ethanol conversion. *Nat Commun*. 2025;16:2073.

   doi: 10.1038/s41467-025-57221-x

4. Liu B, Meng K, Cheng B, Wang L, Liang G, Bie C. Prolonging charge carrier lifetime in s-scheme heterojunctions via ligand-to-metal charge transfer of Ni-MOF for photocatalytic H_2 production and simultaneous benzylamine coupling. *J Mater Sci Technol*. 2025;231:286-295.

   doi: 10.1016/j.jmst.2025.02.013

5. Ju C, Li K, Xu C, Bao F. Challenges and opportunities of hydrogen energy application in public transportation in the post-epidemic period. *Humanit Soc Sci Commun*. 2025;12:283.

   doi: 10.1057/s41599-024-04089-9

6. Wu S, Jiang Y, Luo W, *et al*. Ag-Co_3O_4-CoOOH-nanowires tandem catalyst for efficient electrocatalytic conversion of nitrate to ammonia at low overpotential via triple reactions. *Adv Sci*. 2023;10(33):e2303789.

   doi: 10.1002/advs.202303789

7. Ya Y, Xu YS, Elbanna AM, Liu Y, Sun B, Cheng X. Review of direct ammonia solid oxide fuel cells: Low temperature cell structure and ammonia decomposition strategies. *Renew Sustain Energy Rev*. 2025;213:115350.

   doi: 10.1016/j.rser.2025.115350

8. Gong Z, Wang H, Li C, *et al*. Progress in the design and performance evaluation of catalysts for low-temperature direct ammonia fuel cells. *Green Chem Eng*. 2025;6:54-67.

   doi: 10.1016/j.gce.2024.06.001

9. Zhang C, Hwanga SY, Peng Z. Shape-enhanced ammonia electro-oxidation property of a cubic platinum nanocrystal

catalyst prepared by surfactant-free synthesis. *J Mater Chem A*. 2013;1:14402-14408.

doi: 10.1039/c3ta13641h

10. Zhong C, Hu WB, Cheng YF. On the essential role of current density in electrocatalytic activity of the electrodeposited platinum for oxidation of ammonia. *J Power Sources*. 2011;196:8064-8072.

doi: 10.1016/j.jpowsour.2011.05.058

11. Liu J, Chen B, Kou Y, *et al*. Pt-decorated highly porous flower-like ni particles with high mass activity for ammonia electro-oxidation. *J Mater Chem A*. 2016;4:11060-11068.

doi: 10.1039/c6ta02284g

12. Vooys ACAD, Koper MTM, Santen RA, Veen JARV. The role of adsorbates in the electrochemical oxidation of ammonia on noble and transition metal electrodes. *J Electroanal Chem*. 2001;506:127-137.

doi: 10.1016/S0022-0728(01)00491-0

13. Katayama Y, Okanishi T, Muroyama H, Matsui T, Eguchi K. Enhancement of ammonia oxidation activity over Y_2O_3-modified platinum surface: Promotion of $NH_{2,ad}$ dimerization process. *J Cat*. 2016;344:496-506.

doi: 10.1016/j.jcat.2016.10.020

14. Okanishi T, Katayama Y, Muroyama H, Matsui T, Eguchi K. SnO_2-modified pt electrocatalysts for ammonia-fueled anion exchange membrane fuel cells. *Electrochim Acta*. 2015;173:364-369.

doi: 10.1016/j.electacta.2015.05.066

15. Katayama Y, Okanishi T, Muroyama H, Matsui T, Eguchi K. Electrochemical oxidation of ammonia over rare earth oxide modified platinum catalysts. *J Phys Chem C*. 2015;119:9134-9141.

doi: 10.1021/acs.jpcc.5b01710

16. Zhang HM, Wang YF, Kwok YH, Wu ZC, Xia DH, Leung DYC. A direct ammonia microfluidic fuel cell using nicu nanoparticles supported on carbon nanotubes as an electrocatalyst. *Chemsuschem*. 2018;11:2889-2897.

doi: 10.1002/cssc.201801232

17. Jin Y, Liu Y, Wu RY, Wang J. Local tensile strain boosts the electrocatalytic ammonia oxidation reaction. *Chem Commun*. 2024;60:1104-1107.

doi: 10.1039/d3cc04820a

18. Zhang H, Chen W, Wang H, *et al*. A core-shell NiCu@ NiCuOOH 3D electrode induced by surface electrochemical reconstruction for the ammonia oxidation reaction. *Int J Hydrogen Energy*. 2022;47:16080-16091.

doi: 10.1016/j.ijhydene.2022.03.139

19. Zhu M, Yang Y, Xi S, *et al*. Deciphering NH_3 adsorption kinetics in ternary Ni-Cu-Fe oxyhydroxide toward efficient ammonia oxidation reaction. *Small*. 2021;17:e2005616.

doi: 10.1002/smll.202005616

20. Ren S, Duan D, Wu Y, Zhang H, Ge X. One-step fabrication of free-standing copper/nickel composites for efficient electrocatalytic ammonia oxidation by bimetallic synergistic effect. *Mater Today Commun*. 2025;42:111120.

doi: 10.1016/j.mtcomm.2024.111120

21. Wang J, Qing S, Tong X, *et al*. Boron nanoclusters endowed nife layered double hydroxides with efficient bifunction toward ammonia oxidation reaction and hydrogen evolution reaction. *Appl Surf Sci*. 2023;640:158330.

doi: 10.1016/j.apsusc.2023.158330

22. Han Y, Zhang L, Gu J, Qian J, Wang X. Dual performing PtNi alloys nanosheets for electrocatalytic ammonia oxidation reaction and electrochemical detection of ammonia-nitrogen. *J Alloys Compd*. 2025;1010:177286.

doi: 10.1016/j.jallcom.2024.177286

23. Yu T, Liu G, Nie T, *et al*. Pt-loaded cofe-layered double hydroxides for simultaneously driving HER and HzOR. *ACS Cat*. 2024;14:14937-14946.

doi: 10.1021/acscatal.4c03881

24. Lin X, Zhang X, Wang Z, *et al*, Hyperbranched concave octahedron of PtIrCu nanocrystals with high-index facets for efficiently electrochemical ammonia oxidation reaction. *J Colloid Interface Sci*. 2021;601:1-11.

doi: 10.1016/j.jcis.2021.04.068

25. Zhang S, Hu J, Li SFY, *et al*. Electrochemical sensing mechanism of ammonium ions over an Ag/TiO_2 composite electrode modified by hematite. *Chem Commun*. 2023;59:2636-2639.

doi: 10.1039/d3cc00240c

26. Zhang L, Cai H, Han Y, *et al*. Achieving hierarchical $Co(OH)_2$ nanosheets and Pt nanospheres for high-performance electrochemical detection of ammonia-nitrogen. *Microchem J*. 2025;208:112478.

doi: 10.1016/j.microc.2024.112478

27. Zhang H, Wang H, Tong X, *et al*. Sulfur induced surface reconfiguration of Ni_1Cu_3-S-T/CP anode for high-efficiency ammonia electro-oxidation. *Chem Eng J*. 2023;452:139582.

doi: 10.1016/j.cej.2022.139582

28. Fang H, Liao C, Cai Q, *et al*. Tuning surficial atomic configuration of Pt-Ir catalysts for efficient ammonia oxidation and low-temperature direct ammonia fuel cells. *Chem Eng Sci*. 2023;280:118836.

doi: 10.1016/j.ces.2023.118836

29. Zhang L, Yuan M, Wang X, Gu J. Enhanced electrocatalytic

oxidation activity of platinum-poly(methylene blue) as a sensitive sensor for ammonia-nitrogen detection. *Microchem J*. 2024;199:110238.

doi: 10.1016/j.microc.2024.110238

30. Zhang L, Ma X, Liu J, *et al*. Achieving Ni@(Pt/Ni(OH)$_2$) ternary nanoflowers derived from ni nanoflowers for electrochemical ammonia-nitrogen detection in the aqueous environment. *Microchem J*. 2024;200:110401.

doi: 10.1016/j.microc.2024.110401

31. Wang X, Gong Y, Cai H, *et al*. Fabrication of platinum-decorated NiCo-layered double hydroxide nanoflowers for electrocatalytic ammonia oxidation reaction. *Catalysts*. 2024;14(9):559.

doi: 10.3390/catal14090559